

Implementation of the quantum Fourier transform on a hybrid qubit-qutrit NMR quantum emulator

Shruti Dogra,^{*} Arvind,[†] and Kavita Dorai[‡]

*Department of Physical Sciences, Indian Institute of Science Education & Research Mohali,
Sector 81 Mohali, Manauli PO 140306 Punjab India.*

The quantum Fourier transform (QFT) is a key ingredient of several quantum algorithms and a qudit-specific implementation of the QFT is hence an important step toward the realization of qudit-based quantum computers. This work develops a circuit decomposition of the QFT for hybrid qudits based on generalized Hadamard and generalized controlled-phase gates, which can be implemented using selective rotations in NMR. We experimentally implement the hybrid qudit QFT on an NMR quantum emulator, which uses four qubits to emulate a single qutrit coupled to two qubits.

I. INTRODUCTION

The size of a quantum register can be increased either by increasing the number of qubits (in the standard model of a quantum computer) or by increasing the number of accessible logical states in each quantum element i.e by using qudits (quantum digits) [1–5]. For qudit computing to become a reality, it is essential to concretize the theoretical framework for computation in terms of a set of quantum gates that are universal and can implement any algorithm efficiently. It is however not always straightforward to generalize a qubit gate to the qudit scenario and in some cases, more than one kind of generalization is possible, each retaining some features of the original qubit gate [6]. A gate library for qudits has been proposed, containing one-qudit and two-qudit gates such as the CINC gate, generalized SWAP and general controlled-X (GCX) gates [7–11]. Several qudit computing proposals using different physical systems have been designed to incorporate “hybrid” qudits of different dimensions [12–14], wherein multi-qudit gates are generalized to transform two or more qudits of different dimensions. A set of hybrid quantum gates have been designed to act on qudits of different dimensions, including the hybrid SUM, SWAP, Toffoli and Fredkin gates [15, 16]. Qudits have been used as a resource in secure quantum communication [17], quantum key distribution [18], quantum computing [19] and quantum cloning [20].

NMR has been a fruitful testbed for implementing quantum information processing ideas and is now increasingly being used to manipulate qudits. NMR qudit implementations include using quadrupolar nuclei oriented in a liquid crystal [21] for information processing, studying the dynamics of nonclassical correlations [22] and finding the parity of a permutation using a single qutrit [23] and a single ququart [24]. Logic gates and pseudopure states for a ququart have been implemented using ^{23}Na and ^7Li nuclei oriented in a liquid-crystalline matrix [25, 26].

The quantum Fourier transform (QFT) needs to be specifically tailored for qudit computers as it plays a key role in several quantum algorithms such as factorization [27], quantum phase estimation [28] and the hidden subgroup problem [29]. An efficient decomposition of the QFT for qubits achieves an exponential speedup over the classical fast Fourier transform [30], and has been experimentally implemented by several groups on different physical systems [31–35]. Decompositions of the QFT for qudit systems have been worked out by several groups [36–39].

In NMR systems with “strong” spin-spin coupling terms in the Hamiltonian, the identification of spins as qubits becomes problematic. In such cases, quantum gates have been implemented by selectively manipulating individual transitions between pairs of energy levels [40, 41]. Such “effective” qubits have been constructed by a mapping to the non-degenerate energy eigenstates of a single qudit and have been experimentally demonstrated by partially orienting a ^{133}Cs nuclear spin ($S=7/2$) in a liquid-crystalline medium [42–44]. We carry these ideas forward by carving out a system of two qubits and a qutrit (henceforth referred to as a QQT system) out of four qubits (henceforth referred to as a QQQQ system). Specifically we use the four coupled qubits of 5-Fluorotryptophan to emulate a hybrid system of two qubits and a qutrit (a $2 \otimes 2 \otimes 3$ dimensional Hilbert space). The qubit architecture of 5-Fluorotryptophan due to its specific spin-spin coupling strengths and molecular symmetries, gives rise to twenty lines in the NMR spectrum instead of thirty two lines expected for the non-overlapping energy levels of four qubits. This matches the spectrum expected for a system of two qubits coupled to a qutrit. This system obviously cannot be used as a full-fledged QQQQ system of four qubits due to the degeneracy of transitions. However, by re-labeling and creating a mapping of corresponding energy levels, we are able to show that this QQQQ system can indeed emulate a QQT system and that the allowed non-degenerate transitions are sufficient to implement the required quantum gates.

In this paper we describe a decomposition of the hybrid qudit QFT, using a set of generalized Hadamard and generalized hybrid controlled-rotation gates. The

^{*} shrutidogra@iisermohali.ac.in

[†] arvind@iisermohali.ac.in

[‡] kavita@iisermohali.ac.in

scheme is general and can be implemented on any physical hardware for a hybrid qudit quantum computer. We implement the hybrid QFT on a QQT system (using the four qubits of 5-Fluorotryptophan as a QQT emulator). The requisite hybrid qudit gates can be realized in NMR using selective rotations. Partial state tomography of the final state was achieved by a set of 19 specially designed experiments to reconstruct desired portions of the Hilbert space. The results of the tomography demonstrate the success of the mapping of the QQT system onto the QQQQ system as well as the implementation of the hybrid qubit-qudit QFT on the system.

The material in this paper is organized as follows: Section II describes the basic gates required for quantum computing with qudits and the circuit decomposition of the qudit QFT. Section III describes the experimental implementation of a hybrid qubit-qudit QFT on a four-qubit NMR quantum emulator. Section IV contains some concluding remarks.

II. QFT DECOMPOSITIONS

The state of a system of N hybrid qudits each of a different dimension d_p ($p = 1 \cdots N$) can be written in terms of an orthonormal basis of product states

$$\begin{aligned} |x\rangle &= |x_0\rangle \otimes |x_1\rangle \otimes \cdots \otimes |x_{N-1}\rangle \\ &\equiv |x_0 \cdots x_j \cdots x_k \cdots x_{N-1}\rangle \end{aligned} \quad (1)$$

where $x_j \in \{0, 1, \dots, d_p\}$. For $d_p = d = 2$, this reduces to an N qubit state, with $x = \sum_{j=0}^{N-1} x_j 2^j$, and $x_j \in \{0, 1\}$ being binary integers. However, x does not retain this simple form for hybrid qudits with $d_p > 2$.

A. Qudit Gates

The Fourier gate (F_p) is a single-qudit gate that creates a superposition of all basis states of the qudit, with equal amplitudes, with its action on the p^{th} qudit in an N -qudit system given by [15, 36]:

$$\begin{aligned} F_p |x_j\rangle &= \frac{1}{\sqrt{d}} \sum_{y_k=0}^{d-1} \exp\left(\frac{2\pi i x_j y_k}{d}\right) |y_k\rangle \\ x_j, y_k &\in [0, 1, 2, \dots, (d-1)] \end{aligned} \quad (2)$$

For $d = 2$ (qubit) and $d = 3$ (qutrit) the Fourier gate reduces to the Hadamard gate (H) and the Chrestenson gate (C) respectively:

$$\begin{aligned} H &= \frac{1}{\sqrt{2}} \begin{pmatrix} 1 & 1 \\ 1 & -1 \end{pmatrix} \\ C &= \frac{1}{\sqrt{3}} \begin{pmatrix} 1 & 1 & 1 \\ 1 & e^{\frac{2\pi i}{3}} & e^{\frac{4\pi i}{3}} \\ 1 & e^{\frac{4\pi i}{3}} & e^{\frac{2\pi i}{3}} \end{pmatrix} \end{aligned} \quad (3)$$

For a system of N ‘‘hybrid’’ qudits, each of different dimensions d_1, d_2, \dots, d_N , the action of a two-qudit hybrid

controlled-rotation gate $R_{j,k}^H$ (with j being the control qudit and k the target qudit) is given by [15, 16]:

$$\begin{aligned} R_{j,k}^H |x_0 \cdots x_j \cdots x_k \cdots x_{N-1}\rangle &= \\ \exp\left(\frac{-2\pi i x_j x_k}{\prod_{p=j}^k d_p}\right) |x_0 \cdots x_j \cdots x_k \cdots x_{N-1}\rangle \end{aligned} \quad (4)$$

where d_p is the dimension of the p^{th} qudit; $k > j$ has been assumed here, in order to explicitly define the action of the gate on the N -qudit basis state, however interchanging j and k does not alter the gate operation. For $d_p = d = 2$, the hybrid two-qudit controlled-rotation gate reduces to the standard two-qubit controlled-rotation gate $R_{j,k}$.

B. Hybrid Qudit QFT

The action of the QFT on the basis vectors of a hybrid qudit system is given by [15, 36]:

$$\text{QFT} |x\rangle = \frac{1}{\sqrt{D}} \sum_{k=0}^{N-1} \exp\left(\frac{2\pi i x y}{D}\right) |y\rangle \quad (5)$$

where the states $|y\rangle$ have the same form as $|x\rangle$.

The circuit for implementing the QFT on N hybrid qudits can be decomposed as a set of single-qudit Fourier gates interspersed with two-qudit controlled-rotation gates:

$F_1 R_{1,2}^H R_{1,3}^H \cdots R_{1,N}^H F_2 R_{2,3}^H \cdots F_{N-1} R_{N-1,N}^H F_N$. For N qudits each of a different dimension d_j , the total dimension of the Hilbert space is $D = \prod_{j=1}^N d_j$, and it has to be kept in mind while implementing hybrid controlled-rotation gates that the dimensions of the control and target qudits may be different. After the implementation of the QFT using the above decomposition, the bit values of the resultant state appear in the reverse order. A sequence reversal can be achieved either by applying a series of multi-valued permutation gates [6] or by reading off the result in the reverse order.

III. NMR IMPLEMENTATION

A. The hybrid QQT system

We consider a QQT system with a Hamiltonian governed by [45, 46]

$$\begin{aligned} H^{\text{QQT}} &= \omega_1 I_{1z} + \omega_2 I_{2z} + \Omega_3 I_{3z} + D_Q (3I_{3z}^2 - I^2) \\ &\quad + J_{12} I_{1z} I_{2z} + J'_{23} I_{2z} I_{3z} + J'_{13} I_{1z} I_{3z} \end{aligned} \quad (6)$$

where 1, 2 and 3 label the qubits and the qutrit respectively, I_{iz} is the z -component of the magnetization vector of the i^{th} qubit(qutrit), $I^2 = \sum_i I_{3i}^2$, $i = x, y, z$ is the total magnetization of the qutrit, and $\omega_1, \omega_2, \Omega_3$ denote

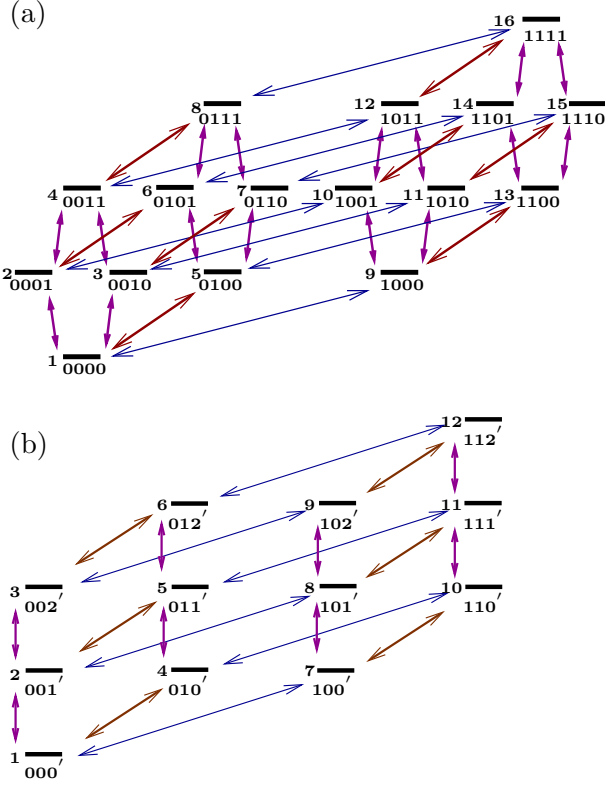


FIG. 1. Energy level diagrams: (a) For a QQQQ system showing 16 energy levels corresponding to four coupled spin-1/2 particles. Spin states are given below each energy level, 0 and 1 correspond to spin states $+\frac{1}{2}$ and $-\frac{1}{2}$ respectively. There are 32 transitions originating from single spin flips. Transitions belonging to spins 1 and 2 are shown in blue and brown respectively while transitions belonging to spins 3 and 4 are shown in purple. (b) For a hybrid QQT system showing 12 energy levels and 20 transitions with energy levels labeled in the computational basis; 0', 1' and 2' correspond to the qutrit spin states +1, 0 and -1 respectively. Each qubit undergoes six single spin flips shown in blue (spin 1) and brown (spin 2) respectively. Qutrit transitions are shown in purple.

their Larmor frequencies i.e. the free precession of the qubits(qutrit) in a static magnetic field. D_Q represents the effective quadrupolar splitting of the qutrit levels and the corresponding term in the Hamiltonian accounts for the static first-order quadrupolar interaction. J_{ij} s denote the strength of the scalar coupling interactions between i^{th} and j^{th} qubits, and J'_{ij} represents an interaction term involving the qutrit.

The QQT Hamiltonian in Eqn. (6) can be emulated by four qubits such that two of the qubits mimic a three-level system. We use spins 3 and 4 of our four-qubit system to mimic a qutrit, such that the qutrit subspace containing levels 1,2 is emulated by the third qubit and the qutrit subspace with levels 2,3 is emulated by the fourth qubit, with the corresponding chemical shifts: $\omega_3 = \Omega_3 + D_Q$ and $\omega_4 = \Omega_3 - D_Q$.

The Hamiltonian of a four-qubit QQQQ system (as-

suming a specific coupling pattern $J_{13} = J_{14} = J'_{13}$, $J_{23} = J_{24} = J'_{23}$ and $J_{34} = 0$) is given by

$$H^{QQQQ} = \omega_1 I_{1z} + \omega_2 I_{2z} + \omega_3 I_{3z} + \omega_4 I_{4z} + J_{12} I_{1z} I_{2z} + J'_{23} I_{2z} (I_{3z} + I_{4z}) + J'_{13} I_{1z} (I_{3z} + I_{4z}) \quad (7)$$

where I_{iz} represents the z-component of the magnetization vector of the i^{th} spin. The NMR spectrum and multiplet pattern of H^{QQQQ} with the assumed J coupling values resembles the first order NMR spectrum of a QQT system (wherein each qubit multiplet contains six transitions and the qutrit multiplet contains eight transitions). Figure 1 shows the energy level diagram of the four-qubit QQT emulator (energy levels numbered from 1-16) and an actual QQT system (energy levels numbered from 1-12).

We use a 5-Fluorotryptophan molecule to emulate the QQT system, with one ^{19}F and three ^1H nuclei representing the four qubits. The molecular structure and NMR parameters are depicted in Figure 2(a) and the thermal equilibrium 1D NMR spectrum is shown in Figure 2(b). The T_1 and T_2 relaxation times for all four qubits range between 1.17 - 3.96 s and 0.82 - 2.28 s respectively. The line intensities in the coupling pattern of 5-Fluorotryptophan differs slightly from that of the ideal QQT emulator, however hybrid qutrit gates implementation can be emulated on this system by tailoring the J -evolution intervals to obtain the desired angles of rotation. The multiplet pattern and single quantum NMR transitions of the QQT emulator are shown in Figure 3; labels below each spectral line refer to the corresponding transitions as per Figure 1(a). The mapping between the transitions (labeled Q1, Q2, T) of the QQT system and the four-qubit QQT emulator (labeled q1, q2, q3, q4) is given in Table 1. For an ideal QQT emulator, the lines of the i^{th} qubit occurring at $\omega_i \pm J_{i3} \mp J_{i4}$ overlap with each other, while in the 5-Fluorotryptophan molecule, $J_{i3} \neq J_{i4}$ ($i \in [1, 2]$) and the lines occurring at $\omega_i \pm J_{i3} \mp J_{i4}$ are separated by $2 |J_{i3} - J_{i4}|$. However this molecule can emulate a QQT system whenever the intensities of the transitions of the i^{th} spin occurring at $\omega_i \pm J_{i3} \mp J_{i4}$ are equal.

B. Experimental implementation of the QFT

The NMR pulse sequence for the experimental implementation of a hybrid qutrit QFT on the four-qubit QQT NMR emulator is shown in Figure 4. A hybrid controlled-rotation gate $R_{j,k}^H$ (where 'j' is the control-qubit and 'k' is the target qutrit) can be realized by a z-rotation of the qutrit state by an angle $\frac{2\pi x_j x_k}{\prod_{m=j}^k d_m}$ ($j \in [0, 1]$, $k \in [0, 1, 2]$).

For the two qubits mimicking the qutrit, this controlled-rotation can be obtained by rotating both the qubits by the same angle with respect to the control qubit. Chemical shift offsets are chosen such that spins 1 and 2 always remain on resonance.

TABLE I. Mapping between the transition frequencies of a QQT system (labeled Q1, Q2 and T) and a four-qubit QQQQ system (labeled q1, q2, q3, q4) which acts as QQT emulator.

Q1	q1	Q2	q2	T	q3, q4
1-7	1-9	1-4	1-5	1-2	1-3, 2-4
2-8	2-10 & 3-11	2-5	2-6 & 3-7	2-3	1-2, 3-4
3-9	4-12	3-6	4-8	4-5	5-7, 6-8
4-10	5-13	7-10	9-13	5-6	5-6, 7-8
5-11	6-14 & 7-15	8-11	10-14 & 11-15	7-8	9-11, 10-12
6-12	8-16	9-12	12-16	8-9	9-10, 11-12
—	—	—	—	10-11	13-15, 14-16
—	—	—	—	11-12	13-14, 15-16

The action of the QFT in extracting state periodicity can be equally well demonstrated on an initial thermal equilibrium state as on a pseudopure state and we hence implement the QFT on a thermal equilibrium state [31]. Beginning with the thermal equilibrium density operator, the first $(\frac{\pi}{2})_{\mathbf{n}_1}^1$ pulse implements a Hadamard gate on the first qubit. The axis of rotation $\mathbf{n}_1 = \cos \theta_1 \hat{x} + \sin \theta_1 \hat{y}$ (aligned at an angle of $\theta_1 = \frac{\pi}{2} + \frac{5\pi}{6}$ with the x-axis) was chosen to obtain a z -rotation of the first qubit by an angle $\frac{5\pi}{6}$, thereby circumventing the high time cost involved in implementing z -rotations. At this point in the pulse sequence, the qubits 2, 3 and 4 do not have any coherence, and thus single spin z -rotations are redundant in their case. The first evolution period incorporates the controlled-rotation gates $R_{1,2}$ and $R_{1,3}^H$ for a time $\tau_{ij} = \frac{\theta_{ij}}{\pi J_{ij}}$ (θ_{ij} is the desired rotation angle). The evolutions under the scalar coupling J_{12} by an angle $\frac{\pi}{2}$, under the scalar coupling J_{13} by an angle $\frac{\pi}{6}$, and under the scalar coupling J_{14} by an angle $\frac{\pi}{6}$ are achieved simultaneously during the first evolution period. Refocusing pulses are introduced at appropriate points to obtain the desired rotation angles. The next module of the hybrid QFT begins with a $(\frac{\pi}{2})_{\mathbf{n}_2}^2$ pulse that implements a Hadamard gate along with producing an effective z -rotation of $\frac{2\pi}{3}$ on the second qubit (the axis \mathbf{n}_2 is chosen to make an angle of $\theta_2 = \frac{\pi}{2} + \frac{2\pi}{3}$ with the x-axis). This is followed by an evolution under the couplings J_{23} and J_{24} during the second evolution interval. The effect of evolution on the first spin is refocused by a pulse in the middle of the evolution period. The final Hadamard gate on the third and

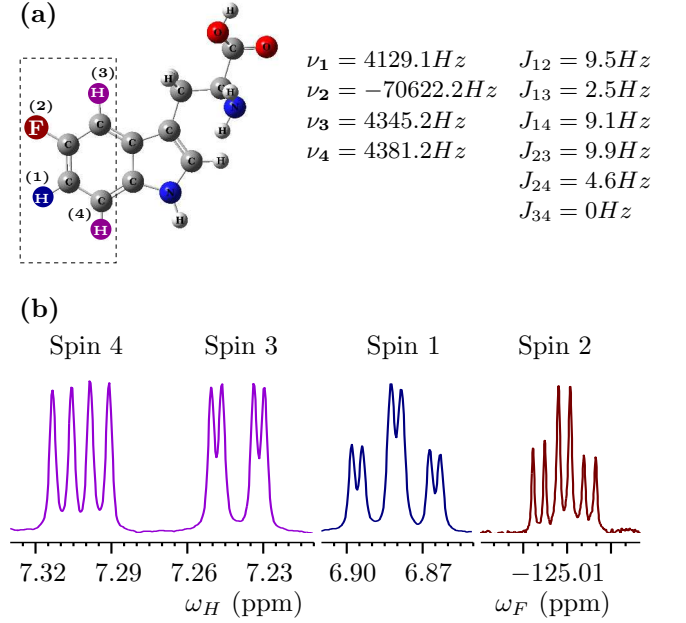


FIG. 2. (a) Molecular structure of 5-Fluorotryptophan with qubits of interest shown in the rectangular block and numbered from 1-4. Three ^1H nuclei and one ^{19}F nucleus form the four-qubit system. The chemical shift values (in ppm) and indirect coupling constants (in Hz) are tabulated alongside. (b) NMR spectrum of the thermal state of 5-Fluorotryptophan. The ^1H and ^{19}F spectra are shown on the same scale. Colors of the spectral lines correspond to the spin color given in the molecular structure. The spins resonate at the frequencies ω_1 , ω_2 and ω_3 , with J_{ij} corresponding to the scalar coupling constant between spins i, j .

fourth qubits is performed by a $(\frac{\pi}{2})_{\mathbf{n}_2}^{3,4}$ pulse (which effectively mimics a single-qutrit Fourier gate). All pulses on qubit 1 are Gaussian pulses of 13 ms duration and the simultaneous excitation of qubits 3 and 4 is achieved using a 7 ms shaped pulse (*Seduce.100*). All the pulses on qubit 2 are hard pulses. Since qubits 3 and 4 are only 36 Hz apart it is difficult to individually address them in an experiment, and hence the controlled-rotation gates on these two qubits have been implemented without applying individual refocusing pulses on them.

C. Tomographic reconstruction

Partial tomography of the QQQQ system was performed in order to reconstruct the desired QQT density matrix. First, a set of operators were designed to reconstruct the full QQT density operator in $d \times d$ dimensional Liouville space (in this case $d = 2 \otimes 2 \otimes 3$). This set of operators was then extended to the analogous set of tomography operations in a 16×16 dimensional operator space of the four-qubit NMR emulator.

The complete characterization of a 12×12 dimensional QQT density operator requires the determination of 143 variables. The 11 diagonal elements (populations) are

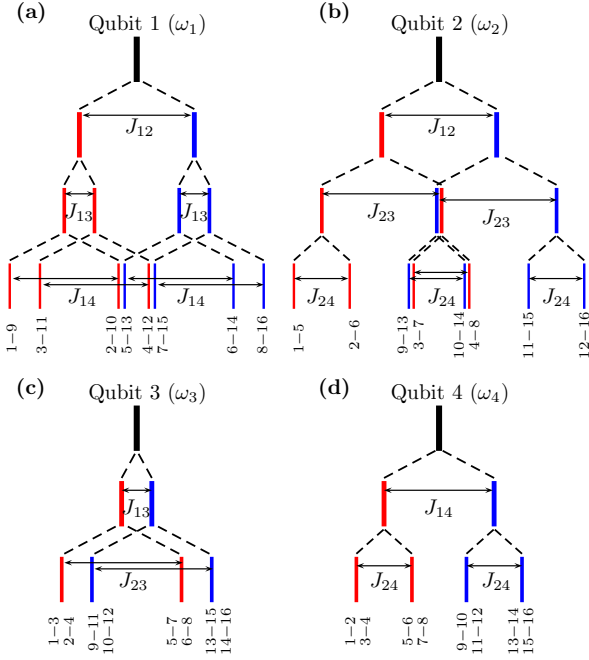


FIG. 3. Multiplet pattern: (a) Of qubit 1, (b) Of qubit 2, (c) Of qubit 3 and (d) Of qubit 4 of the four-qubit NMR emulator. Each multiplet is centered around its chemical shift value (black lines representing $\omega_1, \omega_2, \omega_3$ and ω_4 respectively), which is further split by scalar coupling interaction. The ratio of coupling constants $J_{12} : J_{13} : J_{14}$, $J_{12} : J_{23} : J_{24}$, $J_{13} : J_{23}$ and $J_{14} : J_{24}$ is the same as in the 5-Fluorotryptophan molecule. The line thickness is proportional to the spectral line intensity. Labels below each line refer to the corresponding transition as marked in Figure 1(a).

obtained by applying an appropriate z-gradient to kill off-diagonal elements, followed by spin-selective rotations to project the diagonal elements onto experimentally measurable parts of the density matrix. The remaining 132 elements are obtained by a set of 19 operators: III' , YII' , XII' , IYI' , IXI' , IYI' , IYY' , IXY' , YIY' , XIX' , XXI' , YYI' , XYI' , YXI' , XYY' , XXY' , YXX' , YYX' and IIA' - Grad_z - IYY' , where I is the identity operator, X(Y) refers to a single spin operator and primed operators correspond to qutrit operations. These operators can be implemented by applying the corresponding spin-selective $\frac{\pi}{2}$ pulses (or a no-operation for the identity operator). The last tomography experiment consists of a z gradient pulse sandwiched between two y pulses represented by Λ and Υ applied on the qutrit, of flip angles $(-\frac{\pi}{2})$ and $(\frac{\pi}{4})$ respectively.

A corresponding set of 19 operations can be used to determine the off-diagonal elements of the four-qubit QQQQ system: IIII , YIII , XIII , IYII , IXII , IYYY , IYYY , IXYY , YIYY , XIXX , XXII , YYII , XYII , YXII , XYYY , XXYY , YXXX , YYXX and IIAA - Grad_z - IYYT . The last tomography experiment on the QQQQ system consists of a z gradient pulse sandwiched between two y pulses represented by Λ and Υ , applied simultaneously on qubits 3 and 4 of flip angles $(-\frac{\pi}{2})$ and $(\frac{\pi}{4})$ respectively.

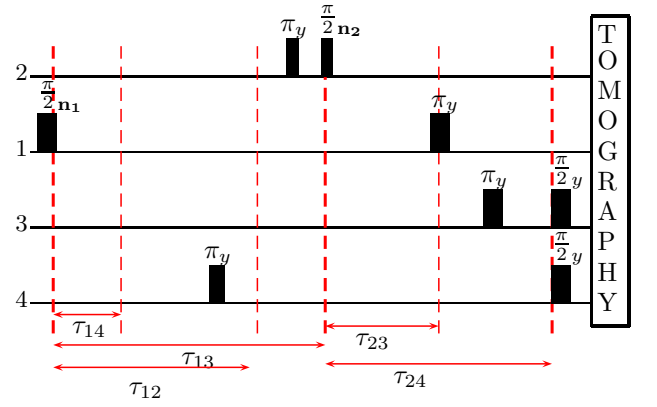


FIG. 4. Pulse sequence for a hybrid QFT on a qubit-qutrit (QQT) system implemented on a four-qubit emulator. Flip angles and axes of rotation are displayed over each pulse. Rotation axes \mathbf{n}_1 and \mathbf{n}_2 are aligned at angles $\theta_1 = \frac{\pi}{2} + \frac{5\pi}{6}$ and $\theta_2 = \frac{\pi}{2} + \frac{2\pi}{3}$ with respect to the x-axis. Thick black rectangles represent selective pulses while thin black rectangles represent non-selective pulses; τ_{ij} s represent time intervals of evolution under the scalar couplings J_{ij} .

The theoretically expected and experimentally obtained tomographs of the real and imaginary parts of the density matrices obtained after applying a hybrid QFT on the four-qubit QQT NMR emulator are given in Figure 5. On visual inspection, one can see that the general pattern of the weights in the density matrices is quite similar, indicating the success of the QFT implementation. Quantitatively, the fidelity of the reconstructed state was computed using the measure [31]:

$$F = \frac{\text{Tr}(\rho_{\text{theory}}^\dagger \rho_{\text{expt}})}{\sqrt{(\text{Tr}(\rho_{\text{theory}}^\dagger \rho_{\text{theory}}))} \sqrt{(\text{Tr}(\rho_{\text{expt}}^\dagger \rho_{\text{expt}}))}} \quad (8)$$

where ρ_{theory} and ρ_{expt} denote the theoretical and experimental density matrices respectively. The fidelity of the experimentally reconstructed density matrix was computed to be 0.83. The loss in fidelity of the experimentally reconstructed state can be attributed to several experimental factors, namely, rf pulse imperfections, imperfect refocusing of chemical shift evolution of unwanted coherences during the evolution intervals, rf field inhomogeneity, and deleterious effects due to spin relaxation. Our experiments point the way to an interesting direction of research in quantum computing with NMR namely, that of using complex coupled qubit topologies to emulate hybrid and higher-dimensional quantum systems.

IV. CONCLUDING REMARKS

It has been proposed that qudit-based quantum computers are able to better optimize Hilbert-space dimensionality and are hence expected to be more powerful than the standard models of qubit quantum computers.

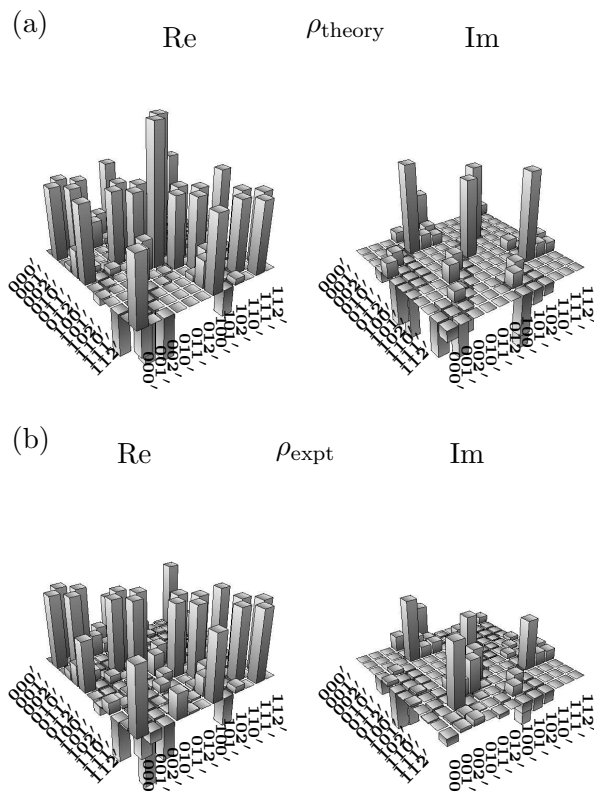


FIG. 5. Tomographs of the real and imaginary parts of the (a) theoretically expected (ρ_{theory}) and (b) experimentally obtained (ρ_{expt}) final density operator obtained after applying a hybrid QFT on the thermal equilibrium state of the four-qubit QQQQ system used as a QQT emulator. The rows and columns encode the computational basis in binary order, from $|000'\rangle$ to $|112'\rangle$.

One of the key quantum circuits in several quantum algorithms is the QFT and it is hence important to look for decompositions of the QFT specifically designed for qudits and hybrid qubit-qudit systems. We used four NMR qubits to emulate a hybrid system of two qubits coupled to a qutrit and implemented the QFT on this hybrid quantum computer. It is expected that these experiments will pave the way for the implementation of full-fledged qudit-based quantum computing proposals.

Acknowledgments All experiments were performed on a Bruker 600 MHz FT-NMR spectrometer in the NMR Research Facility at IISER Mohali. SD acknowledges UGC India for financial support.

-
- [1] A. D. Greentree, S. G. Schirmer, F. Green, L. C. L. Hollenberg, A. R. Hamilton, R. G. Clark, Maximizing the Hilbert space for a finite number of distinguishable quantum states, *Phys.Rev.Lett.* 92 (2004) 097901.
 - [2] B. P. Lanyon, M. H. Barbieri, M. P. Almeida, T. Jennewein, T. C. Ralph, K. J. Resch, G. J. Pryde, J. L. O'Brien, A. Gilchrist, A. G. White, Simplifying quantum logic using higher-dimensional Hilbert spaces, *Nature Phys.* 5 (2009) 134–140.
 - [3] G. K. Brennen, D. P. O'Leary, S. S. Bullock, Criteria for exact qudit universality, *Phys. Rev. A* 71 (2005) 052318.
 - [4] A. B. Klimov, R. Guzmán, J. C. Retamal, C. Saavedra, Qutrit quantum computer with trapped ions, *Phys.Rev.A* 67 (2003) 062313.
 - [5] Q. Lin, B. He, Bi-directional mapping between polarization and spatially encoded photonic qutrits, *Phys. Rev. A* 80 (2009) 062312.
 - [6] A. Muthukrishnan, C. R. Stroud, Multivalued logic gates for quantum computation, *Phys. Rev. A* 62 (2000) 052309.
 - [7] G. K. Brennen, S. S. Bullock, D. P. O'Leary, Efficient circuits for exact-universal computations with qudits, *Quant. Inf. Comp.* 6 (2006) 436.
 - [8] S. S. Bullock, D. P. O'Leary, G. K. Brennen, Asymptotically optimal quantum circuits for d -level systems, *Phys. Rev. Lett.* 94 (2005) 230502.
 - [9] C. M. Wilmott, P. R. Wild, On a generalized quantum swap gate, *Intl. J. Qtm. Inf.* 10 (2012) 1250034.
 - [10] Y.-M. Di, H.-R. Wei, Synthesis of multivalued quantum logic circuits by elementary gates, *Phys.Rev.A* 87 (2013) 012325.
 - [11] J. C. Garcia-Escartin, P. Chamorro-Posada, A swap gate for qudits, *Qtm. Inf. Proc.* 12 (2013) 3625.
 - [12] F. S. Khan, M. Perkowski, Synthesis of multi-qudit hybrid and d -valued quantum logic circuits by decomposition, *Theor. Comp. Sci.* 367 (2006) 336.
 - [13] W.-D. Li, Y.-J. Gu, K. Liu, Y.-H. Lee, Y.-Z. Zhang, Efficient universal quantum computation with auxiliary Hilbert space, *Phys.Rev.A* 88 (2013) 034303.
 - [14] B. Rousseaux, S. Guérin, N. V. Vitanov, Arbitrary qudit gates by adiabatic passage, *Phys.Rev.A* 87 (2013) 032328.
 - [15] J. Daboul, X. Wang, B. C. Sanders, Quantum gates on hybrid qudits, *J.Phys.A* 36 (2003) 2525.
 - [16] D. Gottesman, Fault-tolerant quantum computation with higher-dimensional systems, *Chaos, Solitons and*

- Fractals 10 (1999) 1749.
- [17] H. Bechmann-Pasquinucci, A. Peres, Quantum cryptography with 3-state systems, *Phys.Rev.Lett.* 85 (2000) 3313.
 - [18] S. Groeblacher, T. Jennewein, A. Vaziri, G. Weihs, A. Zeilinger, Experimental quantum cryptography with qutrits, *New J. Phys.* 8 (2006) 75.
 - [19] D. P. O’Leary, G. K. Brennen, S. S. Bullock, Parallelism for quantum computation with qudits, *Phys. Rev. A* 74 (2006) 032334.
 - [20] E. Nagali, D. Giovannini, L. Marrucci, S. Slussarenko, E. Santamato, F. Sciarrino, Experimental optimal cloning of four-dimensional quantum states of photons, *Phys.Rev.Lett.* 105 (2010) 073602.
 - [21] R. Das, A. Mitra, V. S. Kumar, A. Kumar, Quantum information processing by NMR: preparation of pseudopure states and implementation of unitary operations in a single-qutrit system., *Intl. J. Qtm. Inf.* 1 (3) (2003) 387–394.
 - [22] D. O. Soares-Pinto, L. C. Celeri, R. Auccaise, F. F. Fanchini, E. R. deAzevedo, J. Maziero, T. J. Bonagamba, R. M. Serra, Nonclassical correlations in NMR quadrupolar systems, *Phys.Rev.A* 81 (2010) 062118.
 - [23] S. Dogra, Arvind, K. Dorai, Determining the parity of a permutation using an experimental NMR qutrit, *Phys. Lett. A* 378 (2014) 3452.
 - [24] I. A. Silva, B. Cakmak, G. Karpas, E. L. G. Vidoto, D. O. Soares-Pinto, E. R. deAzevedo, F. F. Fanchini, Z. Gedik, Computational speed-up in a single qudit NMR quantum information processor, E-print, [arXiv:1406.3579](#).
 - [25] A. K. Khitrin, B. M. Fung, Nuclear magnetic resonance quantum logic gates using quadrupolar nuclei, *J. Chem. Phys.* 112 (2000) 6963.
 - [26] N. Sinha, T. S. Mahesh, K. V. Ramanathan, A. Kumar, Toward quantum information processing by nuclear magnetic resonance: Pseudopure states and logical operations using selective pulses on an oriented spin 3/2 nucleus, *J. Chem. Phys.* 114 (2001) 4415.
 - [27] P. W. Shor, Polynomial time algorithms for prime factorization and discrete logarithms on a quantum computer, *SIAM J. Comput.* 26 (1997) 1484.
 - [28] R. Cleve, A. Ekert, C. Macchiavello, M. Mosca, Quantum algorithms revisited, *Proc. Roy. Soc. London A.* 454 (1998) 339.
 - [29] D. R. Simon, On the power of quantum computation, *SIAM J. Comput.* 26 (1997) 1474.
 - [30] D. Coppersmith, An approximate Fourier transform useful in quantum factoring, IBM Research Report (1994) RC19642.
 - [31] Y. S. Weinstein, M. A. Pravia, E. M. Fortunato, S. Lloyd, D. G. Cory, Implementation of the quantum Fourier transform, *Phys.Rev.Lett.* 86 (2001) 1889.
 - [32] K. Dorai, D. Suter, Efficient implementations of the quantum Fourier transform: An experimental perspective, *Intl. J. Qtm. Inf.* 3 (2005) 413.
 - [33] H.-F. Wang, X.-X. Jiang, S. Zhang, K.-H. Yeon, Efficient quantum circuit for implementing discrete quantum Fourier transform in solid-state qubits, *J. Phys. B.* 44 (2011) 115502.
 - [34] A.-S. Obada, H. A. Hessian, A.-B. Mohamed, A. H. Homid, Implementing discrete quantum Fourier transform via superconducting qubits coupled to a superconducting cavity, *J. Opt. Soc. Am. B.* 30 (2013) 1178.
 - [35] L. Dong, X.-M. Xiu, H.-Z. Shen, Y.-J. Gao, X. X. Yi, Quantum Fourier transform of polarization photons mediated by weak cross-Kerr nonlinearity, *J. Opt. Soc. Am. B.* 30 (2013) 2765.
 - [36] A. Muthukrishnan, C. R. Stroud, Quantum fast Fourier transform using multilevel atoms, *J. Mod. Opt.* 49 (2002) 2115.
 - [37] V. E. Zobov, A. S. Ermilov, Pulse sequences for realizing the quantum Fourier transform on multilevel systems, *JETP Lett.* 83 (2006) 467.
 - [38] Z. Zilic, K. Radecka, Scaling and better approximating quantum Fourier transform by higher radices, *IEEE Trans. Comp.* 56 (2) (2007) 202–207.
 - [39] Y. Cao, S. G. Peng, C. Zheng, G. L. Long, Quantum Fourier transform and phase estimation in qudit system, *Commun. Theor. Phys.* 55 (2011) 790.
 - [40] T. Gopinath, A. Kumar, Geometric quantum computation using fictitious spin- 1/2 subspaces of strongly dipolar coupled nuclear spins, *Phys.Rev.A* 73 (2006) 022326.
 - [41] J. S. Lee, A. K. Khitrin, Projective measurement in nuclear magnetic resonance, *App. Phys. Lett.* 89 (2006) 074105.
 - [42] A. Khitrin, H. Sun, B. M. Fung, Method of multifrequency excitation for creating pseudopure states for NMR quantum computing, *Phys.Rev.A* 63 (2001) 020301R.
 - [43] K. V. R. M. Murali, N. Sinha, T. S. Mahesh, M. H. Levitt, K. V. Ramanathan, A. Kumar, Quantum-information processing by nuclear magnetic resonance: Experimental implementation of half-adder and subtractor operations using an oriented spin-7/2 system, *Phys.Rev.A* 66 (2002) 022313.
 - [44] A. G. Araujo-Ferreira, C. A. Brasil, D. O. Soares-Pinto, E. R. deAzevedo, T. J. Bonagamba, J. Teles, Quantum state tomography and quantum logical operations in a three qubits NMR quadrupolar system, *Intl. J. Qtm. Inf.* 10 (2012) 1250016.
 - [45] C. P. Slichter, Principles of magnetic resonance, Springer, Newyork, 1996.
 - [46] M. H. Levitt, Spin dynamics : Basics of nuclear magnetic resonance, John Wiley and Sons, Chichester England, 2008.